Versão do arquivo anexado / Version of attached file:

Versão do Editor / Published Version

Mais informações no site da editora / Further information on publisher's website:
https://journals.aps.org/prb/abstract/10.1103/PhysRevB.96.165430

DOI: 10.1103/PhysRevB.96.165430

Direitos autorais / Publisher's copyright statement:

Crystal-field effects in Er^{3+}- and Yb^{3+}-doped hexagonal $NaYF_4$ nanoparticles

A. F. García-Flores,[1] J. S. Matias,[1] D. J. Garcia,[2] E. D. Martínez,[3] P. S. Cornaglia,[2] G. G. Lesseux,[3] R. A. Ribeiro,[1] R. R. Urbano,[3] and C. Rettori[1,3]

[1]*CCNH, Universidade Federal do ABC (UFABC), Santo André, São Paulo 09210-580, Brazil*

[2]*Centro Atómico Bariloche, S.C. de Bariloche, CP8400 Río Negro, Argentina*

[3]*Instituto de Física "Gleb Wataghin", UNICAMP, Campinas, São Paulo 13083-970, Brazil*

(Received 8 September 2017; published 17 October 2017)

Since the up-conversion phenomenon in rare-earths (REs) doped $NaYF_4$ is strongly affected by the crystal electric field (CF), determining the CF parameters, wave functions, and scheme of the energy levels of the RE J multiplets could be crucial to improve and tune the up-conversion efficiency. In this work, the temperature and magnetic field dependent magnetization of $NaY_{1-x}[Er(Yb)]_xF_4$ hexagonal nanoparticles (NPs) is reported. The data were best fit using the appropriated CF Hamiltonian for the $J = 15/2\,(J = 7/2)$ ground state multiplet of Er^{3+} (Yb^{3+}) ions. The B_2^0, B_4^0, B_6^0, and B_6^6 CF parameters were considered in the Hamiltonian for RE ions located at the hexagonal C_{3h} point symmetry site of the $NaYF_4$ host lattice. These results allowed us to predict an overall CF splitting of ~214 (~356 K) for Er^{3+} (Yb^{3+}) and the wave functions and their energy levels for the $J = 15/2$ ($J = 7/2$) ground state multiplet which are in good agreement with the low temperature electron spin resonance experiments. Besides, our measurements allowed us to calculate all the excited CF J multiplets that yield to a good estimation of the up-conversion light emission linewidth. The nonlinear optical light emission of the studied $NaY_{1-x}[Er(Yb)]_xF_4$ hexagonal NPs was also compared with the most efficient up-conversion codoped $NaY_{1-x-y}Er_xYb_yF_4$ hexagonal NPs.

DOI: 10.1103/PhysRevB.96.165430

I. INTRODUCTION

$NaYF_4$ nanoparticles (NPs) doped with rare-earth (RE) ions (Pr, Er, Tm, Yb, etc.) are well known due to their remarkable property of up-conversion, which has led to a diversity of emerging applications nowadays [1–7]. This up-conversion is a nonlinear optical phenomenon where two or more consecutive photons of long wavelength are absorbed leading to the emission of photons with shorter wavelength. The host material $NaYF_4$ can be synthesized in two phases: cubic (namely, α phase) and hexagonal (namely, β phase) [8,9]. The β-phase particles are almost free of defects and present a more intense and therefore more efficient up-conversion emission [10,11] than the α-phase particles [9,12,13]. The RE ions in the host lattice experience an electrostatic potential known as crystal electric field (CF) due to the neighboring charges. The host lattice crystalline structure determines the CF around the dopant ions resulting in distinct optical properties for the NPs [14–16]. Therefore, determining the RE CF levels scheme for the hexagonal doped particles may contribute to understanding the up-conversion emission efficiency. Besides, it is well known that the magnetic response of RE doped materials is significantly affected by the CF, showing a deviation from the expected high temperature (T) Curie-Weiss law at low T. In fact, the CF is responsible for the splitting of the RE ion J multiplet affecting, among other things, the low-T magnetic susceptibility from where the strength of the CF can be determined [17]. In the particular case of RE ions with half-integer spin, the CF splitting always leaves a set of states with Kramers's degeneracy where a magnetic field can lift the time-reversal-symmetry and a microwave transition can be induced via electron spin resonance (ESR).

The aim of this study is to characterize the CF effects of Er and Yb doped $NaYF_4$ hexagonal NPs. A determination of the CF parameters from dc magnetization and ESR measurements is presented here for this NP system.

The point symmetry of the RE ion sites is what determines the parameters that need to be taken into account in the CF Hamiltonian. The crystalline hexagonal NPs have the $P6_3/m$ space group with the RE ions evenly distributed between two distinct sites with C_{3h} and C_1 point symmetries [18]. The C_1 symmetry originates from a slight distortion of the original C_{3h} symmetry. The additional transitions induced by the reduced symmetry in the "C_1" sites are, therefore, expected to have an overall weaker intensity than the ones at the C_{3h} sites. Considering this, from here on we will consider that the whole magnetic response is given by C_{3h} symmetric crystal environment. For a C_{3h} point group symmetry, the CF Hamiltonian for a J multiplet can be written as follows [19]:

$$\mathcal{H}_{CF} = B_2^0 O_2^0 + B_4^0 O_4^0 + B_6^0 O_6^0 + B_6^6 O_6^6, \tag{1}$$

where the B_n^m coefficients are the CF parameters for a given RE and O_n^m are the Stevens's operators which can be expressed in terms of the angular momentum operators J [20,21]. This is the minimum set of parameters that allowed us to explain both ESR and magnetization measurements. In Ref. [18] ten more parameters are added to account for the C_1 symmetry. Our measurements on polycrystalline samples make the additional parameters difficult to determine/differentiate from the ones already introduced for the C_{3h} symmetry.

The CF parameters were determined by fitting the measured powderlike dc-magnetic susceptibility as a function of temperature as well as the field dependent magnetization data at 2 K for both $NaY_{1-x}Er_xF_4$ and $NaY_{1-x}Yb_xF_4$ hexagonal nanoplates. From the best fits to the experimental magnetization data, the obtained CF parameters predict an overall splitting of 214 nm for $NaY_{1-x}Er_xF_4$ and 356 K for $NaY_{1-x}Yb_xF_4$ with anisotropic Kramers's doublets for the ground and excited states. These observations were confirmed by ESR experiments at low T. We find a remarkable

TABLE I. CF parameters B_n^m, actual CF parameters A_n^m, and concentration x for $NaY_{1-x}Er_xF_4$ and $NaY_{1-x}Yb_xF_4$ hexagonal NPs obtained from best fits of the measured dc-magnetization data. ξ relates the average susceptibility $\chi_{avg} = \xi\chi_{\|c} + (1-\xi)\chi_{\perp c}$.

RE ion	ξ	x	B_2^0 (mK)	B_4^0 (mK)	B_6^0 (mK)	B_6^6 (mK)
Er^{3+}	0.55	0.0081	857.04	1.582	0.01728	0.4910
Yb^{3+}	0.60	0.034	9511.92	−70.21	0.6588	0.0555
			A_2^0 (Ka_0^2)	A_4^0 (Ka_0^4)	A_6^0 (Ka_0^6)	A_6^6 (Ka_0^6)
Er^{3+}			506.70	31.64	2.07	59.63
Yb^{3+}			488.79	42.24	1.43	0.12

agreement between the measured up-conversion linewidth and that predicted from the CF results.

II. EXPERIMENT

$NaY_{1-x}Er_xF_4$ and $NaY_{1-x}Yb_xF_4$ NPs with nominal concentrations $x_{Er} = 0.02$ and $x_{Yb} = 0.05$ were synthesized by the chemical decomposition method based on Ref. [8]. From now on, these values will be used to specify the samples studied here, although the estimated concentrations from dc-magnetization measurements are presented in Table I.

Thus, trifluoroacetates $Na(CF_3COO)$ (98%, Aldrich), $Y(CF_3COO)_3$ (99.99%, Aldrich), and $RE(CF_3COO)_3$ (RE = Er, Yb) are used as precursors added to a solution of oleic acid (fluka) and 1-octadecene (90%, Aldrich) in a three-necked flask at room T. All trifluoroacetate precursors were used without any extra purification process. The mixture was heated up to 100 °C to remove any water and oxygen content, with vigorous magnetic stirring in Ar gas flow. Next, the solution was heated up to 330 °C and maintained at that temperature for 30 minutes, always under Ar gas flow. Finally, when the reaction was completed, an excessive amount of absolute ethanol was added into the solution at room T and the NPs were precipitated by a centrifugation process.

The powder x-ray diffraction (XRD) measurements of our $NaYF_4$ NPs were carried out in a Bruker AXS diffractometer with Cu $K\alpha$ radiation ($\lambda = 1.5418$ Å). The NPs morphology and size were characterized by scanning electron microscopy (SEM; FEI Inspect F50, accelerating voltage 30 kV) measurements. The average size of the NPs was obtained by dynamic light scattering (DLS) measurements using a Zetasizer NanoZS equipment. dc-magnetization measurements as a function of temperature (2–300 K) and magnetic field (0–60 kOe) were performed in a SQUID-VSM magnetometer (Quantum Design MPMS3). The continuous wave (cw) ESR measurements were carried out in a Bruker-ELEXSYS 500 spectrometer at X-band frequencies ($\nu = 9.48$ GHz). Powder NP samples dispersed in toluene were placed in a quartz tube inside a TE_{102} resonator coupled to a ^{4}He-flux temperature controller system. Up-conversion emission spectra of powder NPs samples were detected using a QEPro Ocean Optics spectrometer under the excitation of a 980-nm laser diode.

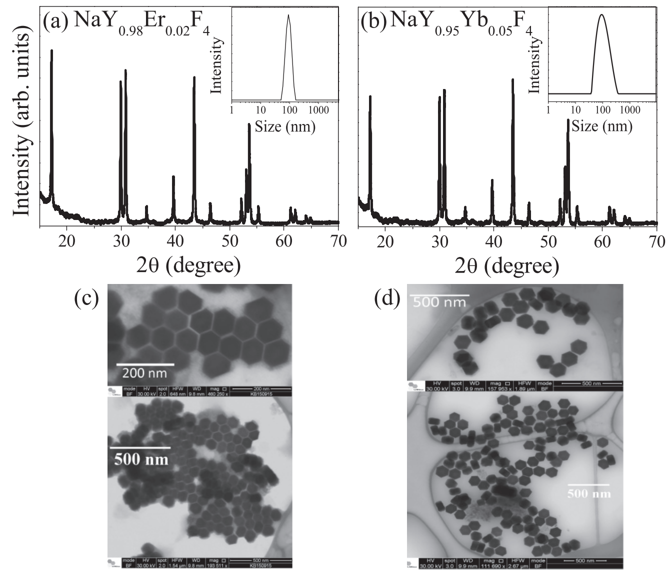

FIG. 1. Powder XRD patterns of (a) $NaY_{0.98}Er_{0.02}F_4$ and (b) $NaY_{0.95}Yb_{0.05}F_4$ NPs. The diffraction peaks were indexed according to the XRD pattern of β-$NaYF_4$. The DLS data are shown in the insets. (c),(d) SEM images of hexagonal nanoplates, corresponding to (a) and (b), respectively.

III. EXPERIMENTAL RESULTS

The powder XRD patterns of our synthesized $NaY_{0.98}Er_{0.02}F_4$ and $NaY_{0.95}Yb_{0.05}F_4$ NPs are shown in Figs. 1(a) and 1(b), respectively. The observed XRD peak

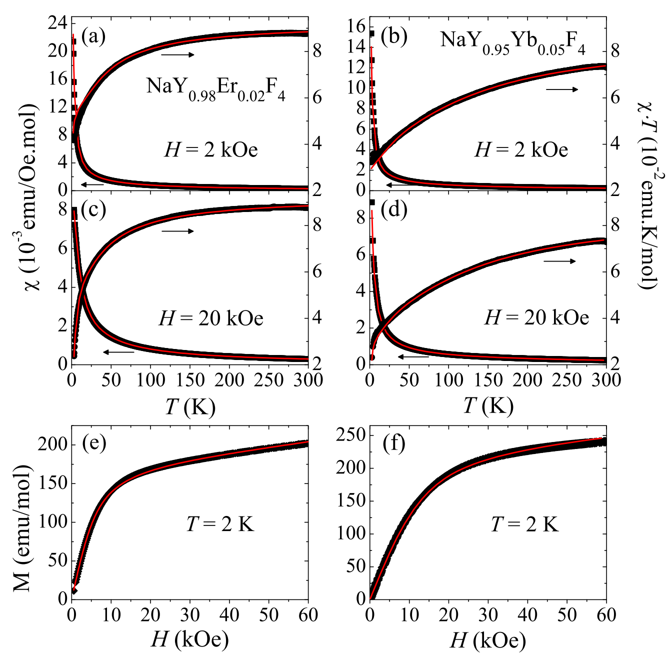

FIG. 2. T dependence of the dc-magnetic susceptibility χ and χT for hexagonal $NaY_{0.98}Er_{0.02}F_4$ and $NaY_{0.95}Yb_{0.05}F_4$ NPs with (a),(b) 2 and (c),(d) 20 kOe; (e),(f) H-dependent magnetization at 2 K. The diamagnetism of the sample holder and the $NaYF_4$ host lattice (-0.62×10^{-4} emu/Oe mol) contribution have been taken into account. The solid red lines are best fits to Eq. (3) in hexagonal symmetry.

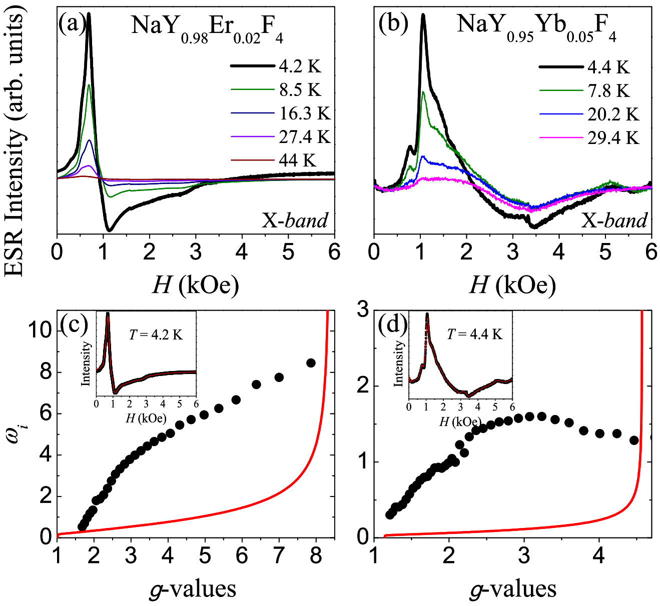

FIG. 3. (a),(b) X-band ESR spectra for different temperatures of hexagonal $NaY_{0.98}Er_{0.02}F_4$ and $NaY_{0.95}Yb_{0.05}F_4$ NPs. (c),(d) The solid red lines represent the expected RE ESR spectral intensity w_i [Eq. (4)] for a *random* distribution of $NaY_{0.98}Er_{0.02}F_4$ and $NaY_{0.95}Yb_{0.05}F_4$ NPs with an anisotropic Kramers's doublet ground state g value obtained from the CF Hamiltonian [Eq. (1)]. The black dots correspond to the deconvoluted g values from the observed ESR spectral intensity at 4.2 K of our *nonrandom* distribution of $NaY_{1-x}RE_xF_4$ NPs. Insets: Experimental (black) and deconvoluted (red) ESR spectra at 4.2 K for Er and Yb of the studied samples.

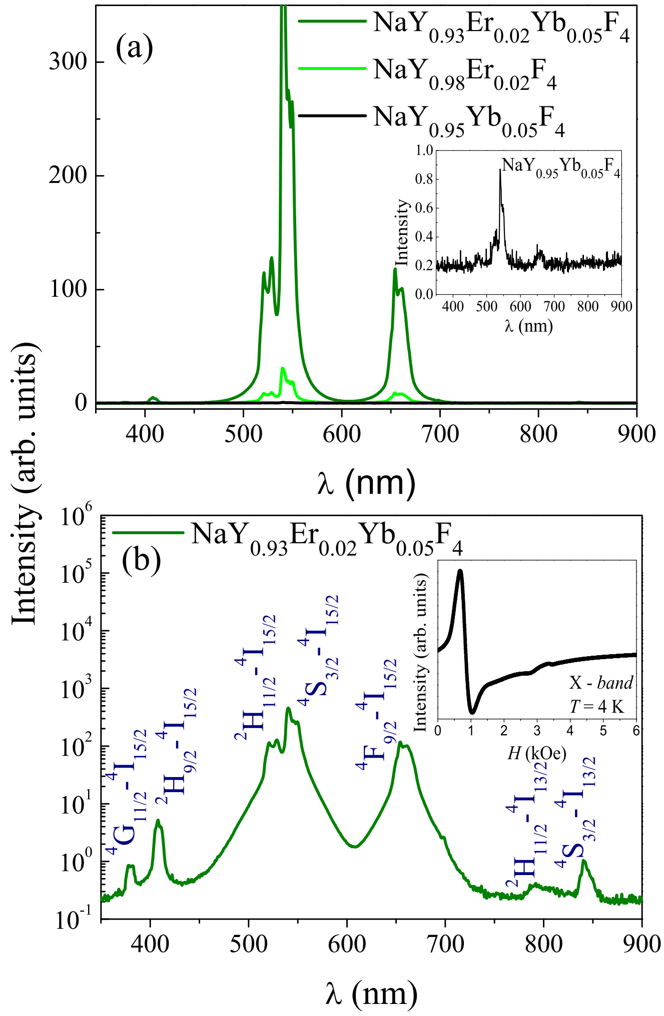

FIG. 4. (a) Light emission spectra of hexagonal $NaY_{0.93}Er_{0.02}Yb_{0.05}F_4$ (olive), $NaY_{0.98}Er_{0.02}F_4$ (green), and $NaY_{0.95}Yb_{0.05}F_4$ (black) NPs excited with a 980-nm laser diode. The inset shows a zoom of the light emission spectrum of $NaY_{0.95}Yb_{0.05}F_4$. (b) For more details, intensity in logarithmic scale of the light emission spectrum of $NaY_{0.93}Er_{0.02}Yb_{0.05}F_4$. Inset: X-band ESR spectrum at 4 K of $NaY_{0.93}Er_{0.02}Yb_{0.05}F_4$.

positions match those previously reported for the β phase [8,11,22]. The average particle size of about 100(20) nm for both $NaY_{0.98}Er_{0.02}F_4$ and $NaY_{0.95}Yb_{0.05}F_4$ were obtained by DLS measurements [inset to Figs. 1(a) and 1(b)]. As one can see, the SEM images presented in Figs. 1(c) and 1(d) show well-defined hexagonal nanoplates (β phase).

Figures 2(a)–2(d) show the dc-magnetic susceptibility χ and χT as a function of temperature for about 10 mg of $NaY_{0.98}Er_{0.02}F_4$ and $NaY_{0.95}Yb_{0.05}F_4$ randomly oriented NPs. The high-T susceptibility presents a Curie-Weiss-like behavior with effective magnetic moments, $\mu = 9.44\,\mu_B$ and $\mu = 4.47\,\mu_B$, corresponding to the oxidation states of Er^{3+} ($4f^{11}$, $J = 15/2$) and Yb^{3+} ($4f^{13}$, $J = 7/2$) ions, respectively. Figures 2(e) and 2(f) present the dc magnetization as a function of magnetic field up to 60 kOe. The measured magnetization was corrected by subtracting the diamagnetic contribution from the sample holder and the host lattice of $NaYF_4$.

Figures 3(a) and 3(b) show the X-band ESR spectra of $NaY_{0.98}Er_{0.02}F_4$ and $NaY_{0.95}Yb_{0.05}F_4$, respectively, at several temperatures. As expected, the ESR intensities behave as Curie-like (i.e., $\propto 1/T$) and show a spectral broadening towards high magnetic fields due to the anisotropy of the Kramers's doublet ground state g value.

Figures 4(a) and 4(b) show the room-T light emission spectra of the $NaY_{0.98}Er_{0.02}F_4$, $NaY_{0.95}Yb_{0.05}F_4$, and $NaY_{0.93}Er_{0.02}Yb_{0.05}F_4$ NPs excited with a 980-nm laser diode.

IV. ANALYSIS AND DISCUSSION

In the presence of an external dc-magnetic field $\vec{H}$, a Zeeman interaction term $\mu_B g_J \vec{H}\cdot\vec{J}$, where g_J is the Landé g factor, μ_B the Bohr magneton, and $\vec{J}$ the total RE angular momentum operator, needs to be added to the CF Hamiltonian of Eq. (1). Therefore, the total Hamiltonian for Er^{3+} or Yb^{3+} ions sited in a hexagonal CF symmetry and under the influence of a uniform dc-magnetic field is given by

$$\mathcal{H} = \mathcal{H}_{CF} + \mu_B g_J \vec{H}\cdot\vec{J}. \tag{2}$$

The energies and the corresponding wave functions of the CF splitted ground multiplet are determined by diagonalizing the Hamiltonian of Eq. (2) for the considered RE ion in terms of the CF parameters B_n^m.

TABLE II. Kramers doublet eigenvalues E_i and associated eigenfunctions φ_i of Er^{3+} ($J = 15/2$) and Yb^{3+} ($J = 7/2$) ions in the hexagonal $NaYF_4$ host lattice.

Ion	E_i(K)	φ_i
Er^{3+}	0	$0.22\lvert\mp 13/2\rangle - 0.86\lvert\mp 1/2\rangle + 0.45\lvert\pm 11/2\rangle$
	3.2	$0.05\lvert\mp 15/2\rangle - 0.82\lvert\mp 3/2\rangle + 0.57\lvert\pm 9/2\rangle$
	6.8	$0.75\lvert\mp 5/2\rangle - 0.66\lvert\pm 7/2\rangle$
	87	$-0.57\lvert\mp 13/2\rangle + 0.26\lvert\mp 1/2\rangle + 0.78\lvert\pm 11/2\rangle$
	108	$-0.07\lvert\mp 15/2\rangle + 0.57\lvert\mp 3/2\rangle + 0.82\lvert\pm 9/2\rangle$
	112	$-0.43\lvert\mp 11/2\rangle + 0.43\lvert\pm 1/2\rangle + 0.79\lvert\pm 13/2\rangle$
	118	$0.55\lvert\mp 5/2\rangle + 0.75\lvert\pm 7/2\rangle$
	214	$0.99\lvert\mp 15/2\rangle + 0.07\lvert\mp 3/2\rangle + 0.03\lvert\pm 9/2\rangle$
Yb^{3+}	0	$\lvert\pm 1/2\rangle$
	119	$\lvert\pm 3/2\rangle$
	264	$\lvert\pm 5/2\rangle$
	356	$\lvert\pm 7/2\rangle$

The magnetization $M(H,T)$ of the J multiplet is given by

$$M(H,T) = \frac{\sum_{i=1}^{2J+1} m_i(H) e^{-E_i(H)/k_B T}}{\sum_{i=1}^{2J+1} e^{-E_i/k_B T}}, \tag{3}$$

where $m_i(H)$ and $E_i(H)$ are the magnetization and energy eigenvalue of each eigenstate. Computing M at a finite H,T using Eq. (3), the CF parameters B_n^m can be obtained by fitting the measured data. Figure 2 presents the magnetic susceptibility and magnetization data together with the corresponding fits (red lines) using Eq. (3). The fits were performed using a single set of B_n^m parameters for each impurity type.

The deviation of the susceptibility data from the expected free ion Curie-Weiss behavior is due to the splitting of the J-multiplet ground state of Er^{3+} or Yb^{3+} under the influence of the CF effect. This deviation is more evident in the product χT shown in Figs. 2(a) to 2(d).

For hexagonal single crystals, the magnetic susceptibility is expected to be anisotropic with components $\chi_{\perp c}$ and $\chi_{\parallel c}$, the c axis being the hexagonal one. For a powder, the measured susceptibility is an average over particle directions $\chi_{\text{avg}} = \xi\ \chi_{\parallel c} + (1-\xi)\chi_{\perp c}$ with $\xi = 1/3$ for a *perfectly random* particle distribution.

In Table I we present the obtained values for ξ, the CF parameters B_n^m, and the RE concentration x resulting from the best fits of the magnetization data for both $NaY_{0.98}Er_{0.02}F_4$ and $NaY_{0.95}Yb_{0.05}F_4$ NPs. It is worth mentioning that ξ differs significantly from 1/3, indicating a preferable orientation of the hexagonal platelets (*nonrandom powderlike*). Therefore, the best fits were achieved with $\xi \sim 0.55$ and $\xi \sim 0.6$ for the Er and Yb doped NPs, respectively.

The obtained CF parameters B_n^m presented in Table I predict an overall CF splitting of about 214 and 356 K for Er^{3+} and Yb^{3+} ions in hexagonal $NaYF_4$ NPs, respectively (see Table II for the wave functions and their energy level diagram scheme in Fig. 5).

Based on Table I it is possible to determine the Kramers's doublet ground state (Table II) and its anisotropic $g_{\parallel c}$ and $g_{\perp c}$ values from the Zeeman splitting, $\Delta E(H) = g\mu_B H$. The expected g values and their anisotropic behavior are shown in Fig. 6 for Er^{3+} and Yb^{3+} ions in single $NaYF_4$ hexagonal NPs.

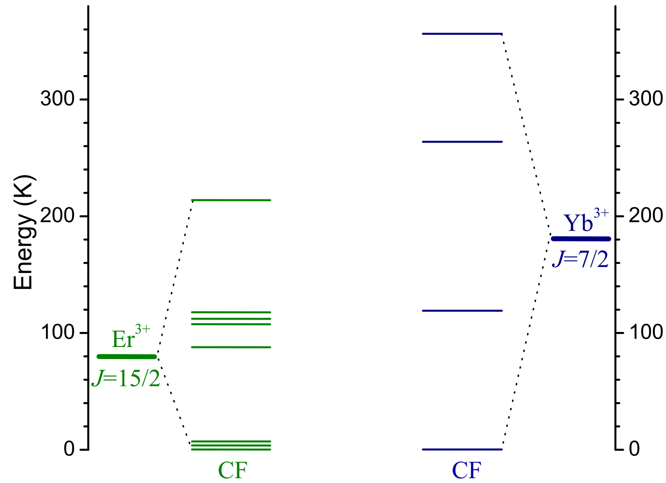

FIG. 5. Schematics of the ground state J multiplet for Er^{3+} and Yb^{3+} due to the CF in the hexagonal $NaYF_4$ host lattice, according to Table II. The narrow bars are Kramers's doublets.

For the C_{3h} symmetry the g values are expected to present a dependence of the azimuthal angle ϕ. However, for the CF parameters determined for this compound it was found to be negligible; see Fig. 6.

Figures 3(a) and 3(b) show the observed powder ESR spectra of $NaY_{0.98}Er_{0.02}F_4$ and $NaY_{0.95}Yb_{0.05}F_4$ NPs at 4.2 and 4.4 K, respectively. It is clear from these wide ESR spectra that they stem from a distribution of resonances that we assume Lorentzian

$$ESR(H) = \sum_i -w_i^2 \frac{2\frac{H-H_i}{\Delta H}}{\left[1+\left(\frac{H-H_i}{\Delta H}\right)^2\right]^2}, \tag{4}$$

where w_i is the ESR intensity associated with a resonance at a field H_i whose linewidth is ΔH. The obtained H_i values allow one to calculate a distribution of g values which is presented in Figs. 3(c) and 3(d) for $\Delta H = 150$ Oe. The solid red lines corresponds to the expected weights ω_i for

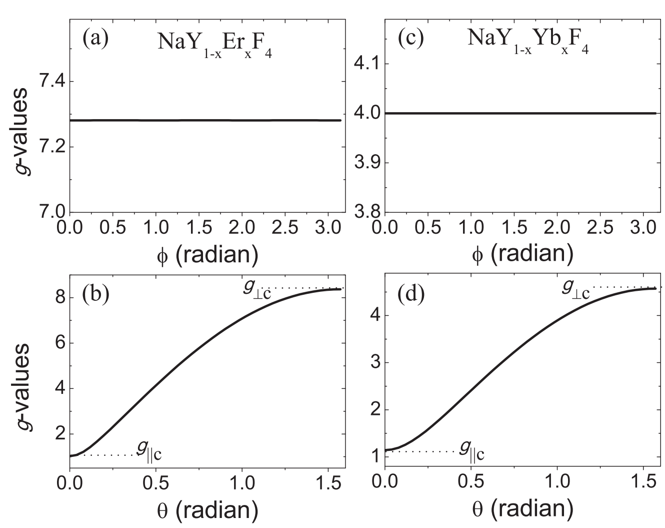

FIG. 6. Angular dependence of the Kramers's doublet ground state g value for the $NaY_{0.98}Er_{0.02}F_4$ and $NaY_{0.95}Yb_{0.05}F_4$ NPs. (a), (b) Polar angle (with respect to the c axis) $\theta = \pi/3$ and azimuthal angle $\phi = 0$ to π. (c),(d) $\phi = 0$ and $\theta = 0$ to $\pi/2$.

TABLE III. Emission maximum linewidth with CF parameters from Er NP's fit in K.

Transition	Theor.	Expt.
$^4F_{9/2} \rightarrow {}^4I_{15/2}$	$218 + 136 = 354 \pm 20$	$\sim 315 \pm 70$
$^4S_{3/2} \rightarrow {}^4I_{13/2}$	$152 + 77 = 229 \pm 20$	$\sim 261 \pm 70$
$^4S_{3/2} \rightarrow {}^4I_{15/2}$	$218 + 77 = 295 \pm 20$	$\sim 520 \pm 70$
$^2H_{11/2} \rightarrow {}^4I_{15/2}$	$218 + 50 = 268 \pm 20$	$\sim 415 \pm 70$
$^2H_{11/2} \rightarrow {}^4I_{13/2}$	$152 + 50 = 202 \pm 20$	$\sim 340 \pm 70$
$^2H_{9/2} \rightarrow {}^4I_{15/2}$	$218 + 93 = 311 \pm 20$	$\sim 585 \pm 70$
$^4G_{11/2} \rightarrow {}^4I_{15/2}$	$218 + 66 = 284 \pm 20$	$\sim 500 \pm 70$

a *completely random* distribution of particle orientations and the CF parameters obtained from the magnetization. These results further corroborate the lack of randomness observed in the dc-magnetic susceptibility data and are consistent with the crystalline NPs oriented predominantly along the c axis.

The CF parameters B_n^m in Eq. (1) are related to the actual lattice CF parameters A_n^m [21]. $B_n^m = \langle r^n \rangle \theta_n A_n^m$, where $\langle r^n \rangle$ is the average over the $4f$ shell and θ_n the geometrical factors ($\theta_2 = \alpha_J$, $\theta_4 = \beta_J$, and $\theta_6 = \gamma_J$ are the second, fourth, and sixth-order Stevens's factors for the RE ion). These parameters are tabulated in Ref. [21] and the values for $\langle r^n \rangle$ were computed in Ref. [23] for free RE ions. In general, the $\langle r^n \rangle$ values depend on the host, whether it is an insulating [24] or a metallic [25] environment. The calculations for these values are beyond the scope of this work. Although the doping at the Y site for Er^{3+}/Yb^{3+} ions may distort the electron density in their neighborhood, the net perturbation should be comparable in both cases. Therefore, the actual CF parameters A_n^m should not depend much on the RE ion itself. Table I shows the relative strengths of the CF parameters A_n^m (in $\mathrm{K}a_0^{-n}$ units where a_0 is the Bohr radius) for the Er^{3+} and Yb^{3+} ions in a hexagonal $NaYF_4$ NPs host lattice. From this table one can observe that the values of the most relevant CF parameters, A_2^0 and A_4^0, are quite comparable for Er^{3+} and Yb^{3+}.

Figure 4 shows the light emission spectra of our samples excited by a 980-nm laser. The observed spectra at room T are compatible with the spectra reported in the literature [12,26,27]. The extremely weak emission observed in the inset of Fig. 4(a) for $NaY_{0.95}Yb_{0.05}F_4$ is compatible with the presence of few ppm of Er^{3+} detected in our ESR experiment at $H \sim 900$ Oe as shown in Fig. 3(b), probably coming from natural impurities in the Y and Yb precursors used in the NPs preparations. On the other hand, the light emission of the codoped $NaY_{1-x-y}Er_xYb_yF_4$ hexagonal NPs confirms the enormous enhancement, relative to the $NaY_{0.98}Er_{0.02}F_4$, of the nonlinear optical efficiency driven by the Yb^{3+} ions. It is worth mentioning that we shall show below the spectral linewidths of the electronic transitions for Er^{3+} are compatible with the overall CF splitting of about 214 K obtained for the ground state of the dopant Er^{3+} ions.

Finally, we use the CF parameters obtained from low energy measurements (magnetization and ESR) to obtain the width of the different optical transitions and compare them with the experimental up-conversion results [see Fig. 4(b) and Table III].

TABLE IV. Single electron CF parameters in K.

RE	b_0^2	b_0^4	b_0^6	b_6^6
Er^{3+}	−14.99	0.1439	−0.008648	−0.2457
Yb^{3+}	−13.31	0.1638	−0.004611	−0.0003885

The energy levels of Er^{3+} obtained using the free-ion (FI) and crystal field interaction are described by the Hamiltonian

$$H = H_{FI} + H_{CF}. \tag{5}$$

Here, the crystal field is given by

$$\mathcal{H}_{CF} = \sum_i b_2^0 O_2^0(i) + b_4^0 O_4^0(i) + b_6^0 O_6^0(i) + b_6^6 O_6^6(i), \tag{6}$$

where i varies over all electrons and the Stevens's operators are for the orbital magnetic momentum of single electrons. Similarly the b_m^n parameters refer to single $l = 3$, $4f$ electron CF parameters. These parameters are related to the ones obtained in a given J multiplet by [20]

$$A_n^m = \frac{1}{\langle r^n \rangle \theta_{J,n}} B_n^m = \frac{1}{\langle r^n \rangle \theta_{l,n}} b_n^m \tag{7}$$

and are presented in Table IV. The free-ion Hamiltonian is

$$H_{FI} = \sum_{k=2,4,6} F^k f_k + \zeta_{4f} \sum_i \vec{l}_i \cdot \vec{\sigma}_i + \alpha L(L+1) + \beta G(R_2) + \gamma G(R_7). \tag{8}$$

The electrostatic interaction is parametrized by $F^{2,4,6}$ (F_0 only modifies the zero of energy) while ζ_{4f} accounts for the spin($\vec{\sigma}_i$)-orbit($\vec{l}_i$) interaction [28]. We include also the configuration interaction terms proportional to α, β, and γ [29]. For simplicity we ignore the three particle terms [30] as this description already leaves the level separation larger than the transition width. From this observation we do not expect the inclusion of those terms to affect the linewidth. All these parameters depend slightly on the environments or approximation used [31–33]. We do not adjust any of these parameters and just use those reported in Ref. [31] for Er^{3+} ions in aqueous solution (see Table V for the parameters used). To obtain the precise energy position of the different levels, a fitting procedure should be used. To show the effect of the CF on the width of the different transitions as determined by low energy measurements (magnetization and ESR) that fitting procedure is not necessary.

The energy levels obtained using the CF for Er^{3+} are presented in Table VI. We also include the approximate experimental level energies. These last values are approximate as the experimental photoemission results from a convolution between the starting and final multiplet. As an approximation for the linewidth (Table III) we use the sum of the level spread of the starting and final multiplets. For example, for the $^4F_{9/2} \rightarrow {}^4I_{15/2}$ transition we assign a width of 136 + 218

TABLE V. Free-ion parameters for Er^{3+} from Ref. [31] in K.

F^2	F^4	F^6	ζ_{4f}	α	β	γ
634.234	96.1542	10.51723	3425.3	26.397	−732.74	934.79

TABLE VI. Excited level positions with CF parameters from Er NPs' magnetic properties fits and experimental estimated positions from photoemission. All energies in K. The zero of energy has been assigned to the ground state $^4I_{15/2}$. For $^4I_{13/2}$ the level position is estimated from the position of the $^4S_{3/2}$ state and the $^4S_{3/2} \rightarrow {}^4I_{13/2}$ absorption.

Transition	Energy (calc.)	Energy (expt.)
$^4I_{15/2}$	0	0
	3	
	6	
	88	
	104	
	113	
	114	
	218	
$^4I_{13/2}$	9380	~9030
	9381	
	9383	
	9424	
	9429	
	9452	
	9532	
$^4F_{9/2}$	21827	
	21857	
	21898	~22000
	21936	
	21963	
$^4S_{3/2}$	26531	~26400
	26608	
$^2H_{11/2}$	27780	
	27789	
	27799	~27460
	27806	
	27818	
	27830	
$^2H_{9/2}$	35331	
	35361	
	35404	~35530
	35420	
	35424	
$^4G_{11/2}$	38149	
	38171	
	38175	~38626
	38187	
	38197	
	38215	

= 354 K. We use the difference between these widths and the ones obtained using the CF parameters for Yb^{3+} impurities (not shown) as a rough estimation for the calculated width error (±20 K). We did not compute a full spectra as the samples are polycrystalline. Nevertheless we checked that the matrix element between the starting and final states is not zero, neither for electric nor magnetic fields polarized on the z direction.

The calculated and computed linewidths agree within the experimental error for almost all energy transitions. The agreement gets worse as the energy of the levels increase (particularly for the $^2H_{9/2} \rightarrow {}^4I_{15/2}$ and $^4G_{11/2} \rightarrow {}^4I_{15/2}$ transitions).

These results confirm that the CF obtained from low energy experiments (magnetization, ESR) provides a good description of the high energy (up-conversion) experiments.

V. SUMMARY

The synthesized $NaY_{1-x}Er(Yb)_xF_4$ NPs presented hexagonal nanoplates morphology (β phase) with 100(20) nm average size. Based on the analysis of our dc magnetization and g values (ESR experiments) for these Yb- and Er-doped $NaYF_4$ NPs, we confirmed that the trivalent RE ions are not superficial but rather incorporated into the lattice of the $NaYF_4$ NPs. In particular, we have obtained the relevant CF parameters for both RE ions Er^{3+} and Yb^{3+} in the hexagonal $NaYF_4$ NPs host lattice from the best fits of the experimental dc-magnetization data. The obtained CF parameters B_n^m predict a CF overall splitting of 214 (356 K) for the $J = 15/2$ ($J = 7/2$) ground state multiplet of Er^{3+} (Yb^{3+}) ions sited in the hexagonal C_{3h} point symmetry. For both studied samples, ESR showed an anisotropic g value in good agreement with those expected for the Kramers's doublet ground state predicted from the analysis of the dc-magnetization data.

The effective CF parameters determined from our magnetic measurements correspond to a C_{3h} symmetry. Previous studies on a related single-crystal of β-$NaGdF_4$:10% Er^{3+} [18] show that the RE ions sit on sites with C_{3h} and C_1 symmetries. High-resolution polarized absorption spectra on this single-crystal taken at 20 K show for the $^4S_{3/2}$ to $^4I_{15/2}$ transition the presence of lines coming from two different sites (A and B). Nevertheless, the deduced width of the $^4S_{3/2}$ level for A and B sites is ~72 and ~75 K, respectively, in very good agreement with our result of ~77 K (see Table VI). The main effect of the presence of two sites is the shift on the energy of the transitions. This effect could explain the larger values of the linewidth with respect to the theoretical calculations at higher energies. Notice also that the CF scheme reported in this work could be improved using other REs as impurities [34].

In conclusion, since the remarkable up-conversion phenomenon of these NPs may be drastically affected by subtle changes in the RE CF local symmetry and energy levels, we strongly believe that the precise determination of the CF parameters is quite important and a challenging step toward optimizing the efficiency of the up-conversion mechanism. In this work, the CF parameters determined through magnetic measurements provide an accurate description of up-conversion experiments.

ACKNOWLEDGMENTS

This work was supported and performed under the auspices of the Brazilian agencies CAPES, CNPq, and FAPESP through Grants No. 2011/19924-2, No. 2012/04870-7, No. 2012/05903-6, and No. 2015/23882-4. The SEM data were acquired in the LNNano at the Centro Nacional de Pesquisa em Energia e Materiais (CNPEM) in Campinas-SP, Brazil. D.J.G. acknowledges support from FONCyT (PICT 2012-1069).

[1] B. Zhou, B. Shi, D. Jin, and X. Liu, Nat. Nanotechnol. **10**, 924 (2015).
[2] A. Shalav, B. S. Richards, and M. A. Green, Sol. Energy Mater. Sol. Cells **91**, 829 (2007).
[3] W. Zou, C. Visser, J. A. Maduro, M. S. Pshenichnikov, and J. C. Hummelen, Nat. Photonics **6**, 560 (2012).
[4] L. Wang, X. Li, Z. Li, W. Chu, R. Li, K. Lin, H. Qian, Y. Wang, C. Wu, J. Li, D. Tu, Q. Zhang, L. Song, J. Jiang, X. Chen, Y. Luo, Y. Xie, and Y. Xion, Adv. Mater. **27**, 5528 (2015).
[5] M. Nyk, R. Kumar, T. Y. Ohulchanskyy, E. J. Bergey, and P. N. Prasad, Nano Lett. **8**, 3834 (2008).
[6] M. Haase and H. Schafer, Angew. Chem. Int. Ed. **50**, 5808 (2011).
[7] J. Zhou, Z. Liu, and F. Li, Chem. Soc. Rev. **41**, 1323 (2012).
[8] H. X. Mai, Y. W. Zhang, R. Si, Z. G. Yan, L. D. Sun, L. P. You, and C. Yan, J. Am. Chem. Soc. **128**, 6426 (2006).
[9] K. Krämer, D. Biner, G. Frei, H. Güdel, M. Hehlen, and S. Lüthi, Chem. Mater. **16**, 1244 (2004).
[10] J. F. Suyver, J. Grimm, M. K. van Veen, D. Biner, K. W. Krämer, and H. U. Güdel, J. Lumin. **117**, 1 (2006).
[11] X. Ye, J. E. Collins, Y. Kang, J. Chen, D. T. N. Chen, A. G. Yodh, and C. B. Murray, Proc. Natl. Acad. Sci. USA **107**, 22430 (2010).
[12] F. Wang and X. G. Liu, J. Am. Chem. Soc. **130**, 5642 (2008).
[13] G. Chen, T. Y. Ohulchanskyy, R. Kumar, H. Ågren, and P. N. Prasad, ACS Nano **4**, 3163 (2010).
[14] G. Blasse and B. C. Grabmaier, *Luminescent Materials*, 1st ed. (Springer, New York, 1994).
[15] L. Wenqin, F. Chengyu, L. Renfu, L. Yongsheng, Z. Haomiao, and C. Xueyuan, Small **7**, 3046 (2011).
[16] F. Auzel, Chem. Rev. **104**, 139 (2004).
[17] W. G. Penney and R. Schlapp, Phys. Rev. **41**, 194 (1932).
[18] A. Aebischer, M. Hostettler, J. Hauser, K. Krämer, T. Weber, H. U. Güdel, and H.-B. Bürgi, Angew. Chem. Int. Ed. **45**, 2802 (2006).
[19] U. Walter, J. Phys. Chem. Solids **45**, 401 (1984).
[20] K. W. H. Stevens, Proc. R. Soc. London, Ser. A **65**, 209 (1952).
[21] M. T. Hutchings, Solid State Phys. **16**, 227 (1964).
[22] F. Wang, Y. Han, C. S. Lim, Y. Lu, J. Wang, J. Xu, H. Chen, C. Zhang, M. Hong, and X. Liu, Nature (London) **463**, 1061 (2010).
[23] A. J. Freeman and R. E. Watson, Phys. Rev. **127**, 2058 (1962).
[24] A. J. Freeman and J. P. Desclaux, J. Magn. Magn. Mater. **12**, 11 (1979).
[25] L. Steinbeck, M. Richter, H. Eschrig, and U. Nitzsche, Phys. Rev. B **49**, 16289 (1994).
[26] D. Gao, X. Zhang, and W. Gao, J. Appl. Phys. **111**, 033505 (2012).
[27] S. Schietinger, L. de S. Menezes, B. Lauritzen, and O. Benson, Nano Lett. **9**, 2477 (2009).
[28] E. U. Condon and G. H. Shortley, *The Theory of Atomic Spectra* (Cambridge University Press, Cambridge, 1951).
[29] K. Rajnak and B. G. Wybourne, Phys. Rev. **132**, 280 (1963).
[30] B. R. Judd, Phys. Rev. **141**, 4 (1966).
[31] W. T. Carnall, P. R. Fields, and K. Rajnak, J. Chem. Phys. **49**, 4424 (1968).
[32] W. T. Carnall, G. L. Goodman, K. Rajnak, and R. S. Rana, J. Chem. Phys. **90**, 3443 (1989).
[33] G. H. Dieke, H. M. Crosswhite, and H. Crosswhite, *Spectra and Energy Levels of Rare Earth Ions in Crystals* (Interscience Publishers, New York, 1968).
[34] D. J. Garcia, F. A. Garcia, J. G. S. Duque, P. G. Pagliuso, C. Rettori, P. Schlottmann, M. S. Torikachvili, and S. B. Oseroff, Phys. Rev. B **78**, 174428 (2008).